Anisotropy-induced polarization mixture of surface acoustic waves in GaN/*c*-sapphire heterostructures

J. Pedrós,* F. Calle, and J. Grajal

Instituto de Sistemas Optoelectrónicos y Microtecnología, Departamento de Ingeniería Electrónica and Departamento de Señales, Sistemas y Radiocomunicaciones, ETSI Telecomunicación, Universidad Politécnica de Madrid, Ciudad Universitaria, 28040 Madrid, Spain

R. J. Jiménez Riobóo

Instituto de Ciencia de Materiales de Madrid-CSIC, Cantoblanco, 28049 Madrid, Spain

Y. Takagaki and K. H. Ploog

Paul-Drude-Institut für Festkörperelektronik, Hausvogteiplatz 5-7, 10117 Berlin, Germany

Z. Bougrioua

Centre de Recherche sur l'Hétero-Epitaxie et ses Applications-CNRS, Bernard Grégory, 06560 Valbonne, France

The characteristics of surface acoustic waves (SAWs) in GaN layers grown on *c*-plane sapphire are investigated. Besides Rayleigh mode, Sezawa and Love modes, which are confined in the nitride layers, arise because of the slow sound propagation in GaN compared with the substrate. In addition, pseudo-SAWs leaking into the bulk are observed. The trigonal crystal symmetry of sapphire not only leads to an anisotropic propagation of the SAWs in the heterostructures, despite the isotropic elastic properties in the *c*-plane GaN, but also mixes their polarization even for the propagation along high-crystal-symmetry directions. Love modes, which are normally piezoelectrically inactive, can be excited by interdigital transducers through this polarization mixture. The nonzero value of the elastic coefficient c_{14} of sapphire is indicated to be the origin of the coupling of sagittal and shear horizontal displacements.

PACS number(s): 68.35.Iv, 68.60.Bs

I. INTRODUCTION

The wide direct band gap together with the strong piezoelectric fields and high chemical inertness of GaN, AlN, and their alloys make them excellent materials for high-power, high-temperature electronic and optoelectronic devices. In this context, violet laser diodes, blue light emitting diodes, and solar blind photodetectors, as well as X-band microwave amplifiers have been successfully developed. Furthermore, these materials present large surface acoustic wave (SAW) velocities, strong electromechanical coupling, and small temperature coefficients of delay.[1] These unique properties are attractive in developing high-frequency SAW devices for signal processing and communication systems. Moreover, new devices have been proposed, in which the optical and electronic properties of the nitrides are modulated by SAWs.[2–6]

Nitride films are typically grown on Si, sapphire, SiC, or diamond substrates. The spectrum of acoustic modes in a heterostructure[7] strongly depends on the mismatch of the elastic properties between the layer and the substrate, since the layer thickness is typically smaller than the penetration depth of the surface waves, which is on the order of the wavelength. The effects are manifested as a dispersion of the acoustic waves and the emergence of various modes. Although wurzite nitrides (crystal class 6mm) present isotropic elastic properties in the *c*-plane, the sixfold-symmetric elastic properties of *c*-sapphire, i.e., (0001)-oriented sapphire, (crystal class $\bar{3}m$) leads to an anisotropic SAW propagation in the nitride layers when sapphire is employed as the substrate.[8–10]

In most heterostructures, in particular when the propagation is along the directions of high crystal symmetry, the wave equations and the boundary conditions lead to two uncoupled sets of solutions.[7] The solutions having only transverse displacement components are called Love modes, whereas those with only sagittal-plane displacements are called Rayleigh-type or simply Rayleigh modes, because of their similarity to the Rayleigh wave in a bulk material. The displacements for all the Love modes and for the Rayleigh modes except the lowest order are confined in the overlayer. They only exist if the bulk transverse velocity in the substrate is higher than in the overlayer (slow-on-fast structure). The higher-order Rayleigh modes are usually called Sezawa modes, in reference to the first Rayleigh-type guided mode discovered by Sezawa.[11]

In this work, the propagation characteristics of various surface and pseudosurface acoustic modes in GaN/sapphire(0001) heterostructures are investigated. The SAW dispersion along the $[11\bar{2}0]$ and $[1\bar{1}00]$ sapphire directions, as well as the anisotropy of the propagation in the heterostructures are experimentally determined and compared with numerical simulations. We differentiate the type of the guided surface modes in terms of Love and Sezawa (Rayleigh-type) modes based on the study of their polarization. We observe an unexpected excitation of shear horizontal (SH) waves, which are piezoelectrically inactive on a bulk GaN crystal. The unusual excitation is revealed to be due to the polarization mixture induced by the nonzero value of the elastic coefficient c_{14} of the trigonal substrate. The coupling
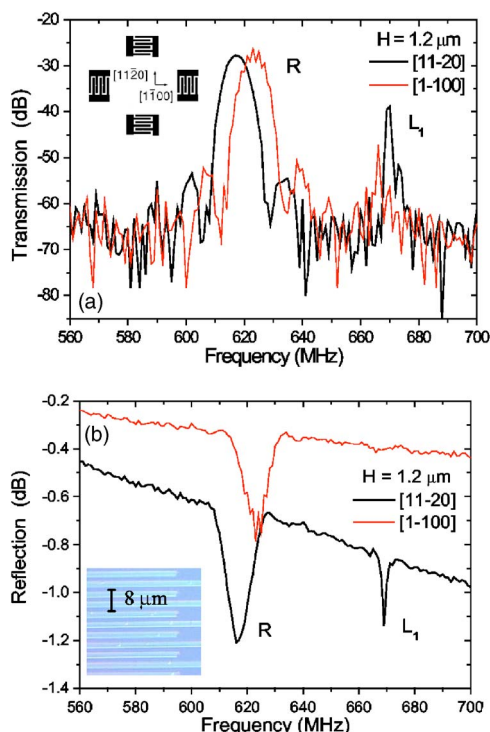
FIG. 1. (Color online) (a) Transmission and (b) reflection characteristics of two SAW filters on a 1.2-μm-thick GaN film along the $[11\bar{2}0]$ and $[1\bar{1}00]$ directions of sapphire. The configuration of the two orthogonal delay lines is illustrated in the inset of (a). The resonances are associated with the Rayleigh (R) and the first Love mode (L_1). The inset of (b) shows a micrograph of the interdigital transducer having a period of 8 μm.

to the Love modes is attractive since it enables us to generate the piezoelectric fields in the nitride layers in the direction transverse to the propagation using SAWs launched by interdigital transducers (IDTs).

II. EXPERIMENT

Nominally undoped GaN epitaxial films were grown on c-sapphire substrates by metal-organic vapor phase epitaxy. The crystal orientation relationships are GaN(0001)∥sapphire(0001) and GaN$[01\bar{1}0]$∥sapphire$[11\bar{2}0]$. The thickness H of the nine GaN films to be employed in this work is in the range of 1–15 μm. The crystal quality of the GaN epilayers was assessed using high resolution x-ray diffraction. The θ-2θ scan revealed the (0002) GaN and the (0006) sapphire reflections. The rocking curve indicated the full-width at half maximum of the peak being approximately 7 arcmin for a 1.2-μm-thick sample, evidencing the high quality of the nitride layer.

Two orthogonal delay lines were defined by contact lithography on the GaN surface along the $[11\bar{2}0]$ and $[1\bar{1}00]$ in-plane directions of sapphire, as shown in the inset of Fig. 1(a). Throughout this paper, we specify the propagation direction of SAWs with respect to the crystal orientation of the sapphire substrates. The simultaneous definition of the two

SAW delay lines in the same lithographic step ensures that they are identical. In order to rule out any differences between the mask patterns of the two delay lines, the SAW characteristics were confirmed to be unchanged under a 90° rotation of the mask. The IDT parameters are as follows: the finger width and the pitch, which are identical for our IDTs, $d=2$ μm, the transducer period $\lambda=4d$ [see the micrograph in the inset of Fig. 1(b)], the finger length 400 μm, and the separation between IDTs 250λ. After the lithography, Ti(10–30 nm)/Al(100–150 nm) bilayers were deposited by electron-beam evaporation. In order to study the angular dispersion of the acoustic modes, the same structures were additionally fabricated for propagation angles tilted from the aforementioned high-symmetry directions. The transfer function of the devices was obtained by means of a coplanar probe station combined with a HP8510C network analyzer.

III. RESULTS AND DISCUSSION

A. Anisotropic propagation

Figures 1(a) and 1(b) show, respectively, the transmission and reflection amplitudes in the two orthogonal SAW delay lines for a 1.2-μm-thick GaN film ($kH=2\pi H/\lambda=0.94$). Two clear resonances appear in the transmission for both of the propagation directions. The lower-frequency peak is associated with the Rayleigh mode (labeled as R), while the other one corresponds to the first Love mode (L_1). The Love mode shows up in the spectra although IDTs are normally unable to excite the SH wave. We will examine in Sec. III B the mechanism behind this unexpected excitation of the L_1 mode. The guided propagation is a consequence of the velocity of the transverse bulk wave in sapphire being higher than in GaN. Both the R and L_1 modes exhibit frequency and amplitude anisotropies between the $[11\bar{2}0]$ and $[1\bar{1}00]$ directions. The insertion loss of the R mode is similar for the two propagation directions. For the L_1 mode, the insertion loss is appreciably higher in the $[1\bar{1}00]$ direction than in the $[11\bar{2}0]$ direction. Correspondingly, the magnitude of the dip in the reflection spectrum due to the L_1 mode is less than the measurement noise for the propagation along the $[1\bar{1}00]$ direction. With respect to the frequency anisotropy, the resonance frequency of the R mode in the $[11\bar{2}0]$ direction is about 6 MHz lower than that in the $[1\bar{1}00]$ direction. The peak shifts to the opposite direction in frequency for the L_1 mode by about 4 MHz.

Figure 2 shows the transmission amplitude in the delay lines when the layer is 1.7 μm thick ($kH=1.33$). While the R mode exhibits an anisotropy similar to that for the 1.2-μm-thick layer, the L_1 mode is observed only in the $[11\bar{2}0]$ direction. The L_1 mode is absent in the spectra along the $[1\bar{1}00]$ direction also when the GaN layer is even thicker. At higher frequencies, additional transmission peaks are observed. As the resonance frequencies imply velocities which are larger than the velocity of the slow transverse bulk wave in sapphire, these peaks are associated with the first pseudo-bulk mode (hence labeled PB_1). These high frequency modes
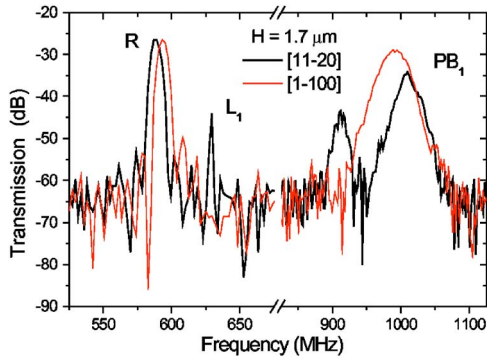
FIG. 2. (Color online) Transmission spectra of two SAW delay lines on a 1.7-μm-thick GaN film along the $[11\bar{2}0]$ and $[1\bar{1}00]$ directions of sapphire. The peaks associated with the Rayleigh mode, the first Love mode, and the first pseudobulk mode are labeled R, L_1, and PB_1, respectively. The SAW wavelength is 8 μm.

TABLE I. Mass density ρ, elastic constants c_{ij}, piezoelectric coefficients e_{ij}, and static dielectric constants ε_{ij} used in the simulations. The values for GaN are taken from Refs. 8 and 22, whereas those for sapphire are from Refs. 14 and 27.

	GaN	Sapphire
ρ (Kg/m^3)	6150	4000
c_{11} (GPa)	370	495.08
c_{12} (GPa)	145	160.52
c_{13} (GPa)	110	114.0
c_{14} (GPa)	0	−22.02
c_{33} (GPa)	390	496.0
c_{44} (GPa)	98	143.17
c_{66} (GPa)	112.5	167.28
e_{15} (C/m^2)	−0.30	0
e_{31} (C/m^2)	−0.36	0
e_{33} (C/m^2)	1.0	0
ε_{11}	8.9	9.34
ε_{33}	8.9	11.54

exhibit a larger frequency shift between the two propagation directions in comparison to that of the R and L_1 modes. This can be understood by the fact that the pseudo-SAWs penetrate deep into the sapphire substrate, which is responsible for the anisotropy. Note that the PB_1 mode splits into two peaks (or accompanies a secondary peak) for the propagation along the $[11\bar{2}0]$ direction. The transmission peaks due to pseudo-SAWs are, in general, broad in frequency, reflecting their bulk-like nature.

The identification of the type of the acoustic modes is based on a comparison of the experimental data with numerical calculations. The simulations were carried out using two methods. The first is based on a Green's function formalism,[12,13] which was developed to calculate the surface Brillouin spectra. In order to simulate the crystal orientations that correspond to the two SAW propagation directions, the effective elastic coefficients of the sapphire were calculated as described in Ref. 14. The second method is based on the transfer matrix approach described in Ref. 15. The crystal orientation and propagation direction of each layer are defined through the Euler angles. The material parameters used in the numerical calculations are listed in Table I.

The results of the simulations for the GaN/sapphire heterostructures are summarized in Figs. 3(a) and 3(b) for the propagation along the $[1\bar{1}00]$ and $[11\bar{2}0]$ directions of sapphire, respectively. The solid lines present the dispersion of SAWs and pseudo-SAWs calculated using the transfer matrix approach. The experimental data (circles) have been determined using the resonance frequency of the IDTs. The gray scale depicts the magnitude of the shear vertical component of a wave having the given values of the velocity and kH calculated using the Green's function formalism. Here the whiter areas indicate larger magnitude. The results of the two simulations are in agreement with each other. We note that the present version of the Green's function-based simulation is not applicable for the Love modes.[12]

The velocity of the Rayleigh mode R decreases from its value in sapphire for $kH=0$, to that in GaN for $kH=\infty$. Additionally, Love modes L_i and Sezawa modes S_i emerge nearly periodically beyond their threshold values of kH. The

velocities of both Love and Sezawa modes decrease monotonically with increasing kH, spanning between the values of a specific bulk velocity in GaN and sapphire. The range is set by the fast bulk transverse velocity v_{FT} for Love modes and by the slow bulk transverse velocity v_{ST} for Sewaza modes. The pseudobulk modes PB_i arise at velocities higher than v_{FT} in sapphire and propagate up to the velocity of the longitudinal bulk wave v_L in the substrate. These fast leaky modes with a predominant longitudinal character when approaching v_L are called high velocity or quasilongitudinal pseudo-SAWs.[16,17] Although pseudosurface waves attenuate as they propagate, the PB_i modes present high transmission amplitudes in the GaN/sapphire structure as shown in Fig. 2 for PB_1. We note, however, that the splitting of this mode when the propagation is along the $[11\bar{2}0]$ direction finds no counterpart in Fig. 3(b).

The symbols in Fig. 4 show the angular dependence of the velocities of the R and L_1 modes within the surface plane for the 1.2-μm-thick GaN film. The anisotropy exhibits a sixfold symmetry originating from the sapphire substrate. The numerical results shown by the lines are in good agreement for the R mode, while the theory overestimates the velocity by about 1% for the L_1 mode. Upon tilting the propagation angle from the $[1\bar{1}00]$ direction toward the $[11\bar{2}0]$ direction of sapphire, the velocity of the R mode decreases whereas that of the L_1 mode increases. Note that the sixfold symmetry implies that the tilt angle of 30° is equivalent to the propagation along the $[11\bar{2}0]$ direction. The opposite shifts in velocity with the tilt angle reflect the fact that the velocities of the R and L_1 modes are related to v_{ST} and v_{FT}, respectively. The two bulk transverse velocities have such angular dependence in sapphire, as summarized in Table II. It should be emphasized that the experimental determination of the angular dependence for the L_1 mode is made possible because of the unusual excitation of the mode in the present system.
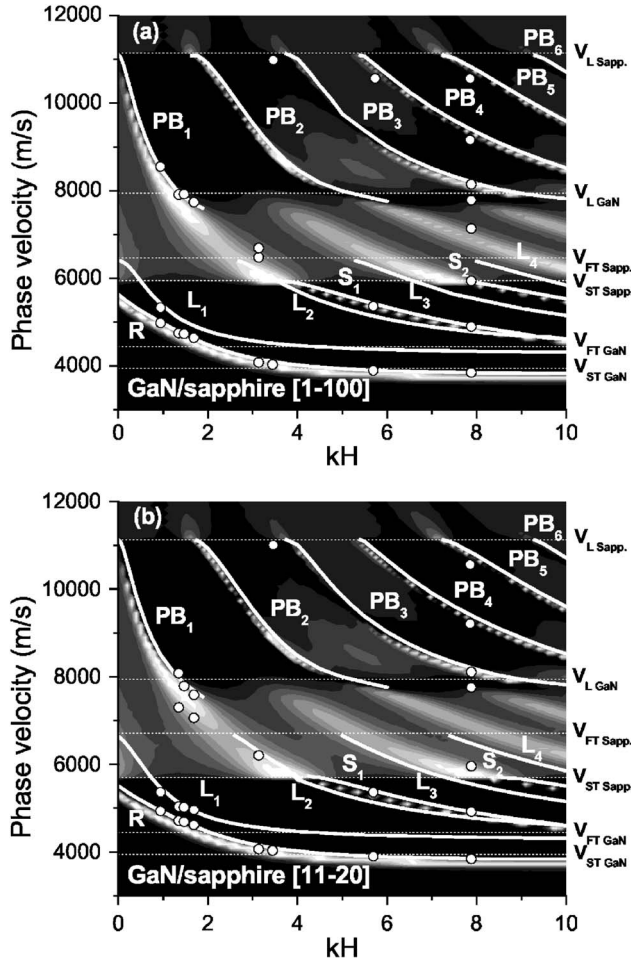
FIG. 3. Surface and pseudosurface modes and their dispersion in the GaN/sapphire structures. The propagation is along the directions (a) $[1\bar{1}00]$ and (b) $[11\bar{2}0]$ of sapphire. The solid lines show the dispersion calculated using the transfer matrix approach. The experimental data are shown by the circles. The gray scale indicates the magnitude of the shear vertical component of the acoustic waves for the values of the velocity and kH calculated using the Green's function formalism. The brighter the scale is, the larger the magnitude. Rayleigh, Sezawa, Love, and pseudobulk modes are denoted R, S_i, L_i, and PB_i, respectively. The dotted lines indicate the longitudinal (v_L) and fast (v_{FT}) and slow (v_{ST}) transverse bulk velocities of the substrate and the overlayer.

The quantitative discrepancy in the velocity of the L_1 mode between the experimental and numerical results may originate from the difference of the material parameters between a bulk and a thin film. The mass density and the elastic coefficients may be modified by the large strain in the nitride films on sapphire substrates. The influence of the strain can be particularly significant for the confined mode L_1. It should be pointed out, however, that a similar systematic discrepancy in the angular dependence of the velocities of SAWs and pseudo-SAWs has been reported for the (111) surface of a GaAs single crystal,[18] which exhibits a sixfold symmetry similar to sapphire(0001). A 2–4 % disagreement was observed, although the single crystal is free from the stress. The deviation was attributed to the difference of the values of the elastic coefficients measured using Brillouin scattering (GHz
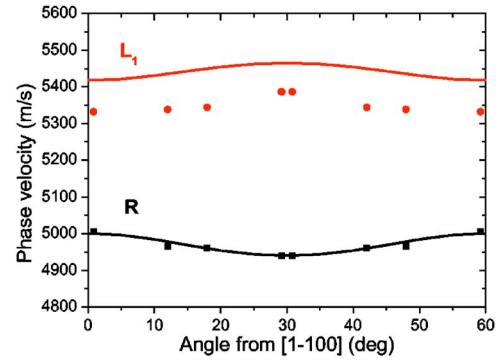

FIG. 4. (Color online) Angular dependence of the velocity of the Rayleigh (R) and first Love (L_1) modes for $kH=0.94$. The symbols show the experimental data, whereas the numerical results are shown by the lines. The propagation angle is defined from $[1\bar{1}00]$ toward $[11\bar{2}0]$. The angle of 30° is equivalent to $[11\bar{2}0]$ due to the sixfold symmetry in the *c*-plane sapphire.

range) and the ultrasonic techniques (MHz range).

B. Polarization mixture

Shear horizontal waves have been observed in GaN(0001)/AlN(0001)/Si(111) structures by Brillouin scattering.[19] The interaction of these modes with light arises from the elasto-optic effect.[20] The possibility of detecting the SH waves depends on the polarization of the light and the scattering geometry. The excitation of Love modes by means of conventional IDTs requires a piezoelectrically active material for these specific modes, such as ST-cut quartz.[21] Although Love modes are piezoelectrically inactive in wurzite nitrides, the L_1 mode was detected in Figs. 1 and 2. For the propagation along the $[11\bar{2}0]$ direction of sapphire, the L_1 mode was observed over a range of kH in the regime of $kH < 2$; see Fig. 3(b). Although the L_1 mode was cumbersome to excite along the $[1\bar{1}00]$ direction, an unmistakable excitation was detected at $kH \approx 1$; see Fig. 3(a). In addition, the L_2 mode was also excited along the $[11\bar{2}0]$ direction at $kH \approx 3$.

The unexpected excitation of Love modes along the high-crystal-symmetry directions is caused by the mixture of the mode polarization induced by the finite value of the elastic coefficient c_{14} of sapphire. Let us consider the acoustic propagation in the individual components of the GaN/sapphire heterostructure. The elastic wave equations for the

TABLE II. Velocities of the slow transverse (v_{ST}), fast transverse (v_{FT}), and longitudinal (v_L) bulk waves, as well as the velocity (v_R) of the Rayleigh wave in *c*-plane GaN and sapphire. The propagation direction is specified for the sapphire.

	v_{ST} (m/s)	v_{FT} (m/s)	v_L (m/s)	v_R (m/s)
Sapphire $[1\bar{1}00]$	5954	6467	11140	5637
Sapphire $[11\bar{2}0]$	5703	6714	11125	5492
GaN	3992	4277	7756	3704

particle displacements u_j along the coordinate axes x_j are intercoupled to the anisotropic Laplace's equation for the potential ϕ by the piezoelectric tensor e_{ijk}. Thus u_j and ϕ must satisfy the following equations in each medium of the layered structures:

$$\rho \frac{\partial^2 u_j}{\partial t^2} - \sum_{ikl} c_{ijkl} \frac{\partial^2 u_k}{\partial x_i \partial x_l} - \sum_{ik} e_{kij} \frac{\partial^2 \phi}{\partial x_i \partial x_k} = 0, \quad (1)$$

$$\sum_{ikl} e_{ikl} \frac{\partial^2 u_k}{\partial x_i \partial x_l} - \sum_{ik} \varepsilon_{ik} \frac{\partial^2 \phi}{\partial x_i \partial x_k} = 0, \quad i,j,k,l = 1,2,3, \quad (2)$$

where ρ is the density, c_{ijkl} is the elastic stiffness tensor, and ε_{ik} is the dielectric permittivity tensor. Solutions of the form

$$u_j = \alpha_j \exp(ikbx_3)\exp[ik(x_1 - vt)], \quad (3)$$

$$\phi = \alpha_4 \exp(ikbx_3)\exp[ik(x_1 - vt)] \quad (4)$$

are assumed, where v is the phase velocity and k is the wave vector component along the propagation direction x_1. The coefficients α_j give the relative amplitudes of the four components and b is a complex number which gives the variation depth of the wave defined in the plane perpendicular to the x_1 axis.

In the case of the (0001) surface of GaN, these equations result in the following expression for any in-plane propagation direction (due to the isotropy of the c-plane GaN):

$$\begin{pmatrix} c_{11} + c_{44}b^2 - \rho v^2 & 0 & (c_{13} + c_{44})b & (e_{15} + e_{31})b \\ 0 & c_{66} + c_{44}b^2 - \rho v^2 & 0 & 0 \\ (c_{13} + c_{44})b & 0 & c_{44} + c_{33}b^2 - \rho v^2 & e_{33}b^2 + e_{15} \\ (e_{15} + e_{31})b & 0 & e_{33}b^2 + e_{15} & -\varepsilon_{11} - \varepsilon_{33}b^2 \end{pmatrix} \begin{pmatrix} \alpha_1 \\ \alpha_2 \\ \alpha_3 \\ \alpha_4 \end{pmatrix} = \begin{pmatrix} 0 \\ 0 \\ 0 \\ 0 \end{pmatrix}. \quad (5)$$

The sagittal components α_1 and α_3 are decoupled from the SH component α_2. Since the potential α_4 is coupled only to the sagittal displacements, no SH mode can be excited through the piezoelectric effect in a bulk GaN.

The acoustic properties in the c-plane of sapphire are not isotropic. We focus here our attention on the propagation along the two high-crystal-symmetry directions $[1\bar{1}00]$ and $[11\bar{2}0]$. The wave equations for propagation along the $[11\bar{2}0]$ sapphire direction are

$$\begin{pmatrix} c_{11} + c_{44}b^2 - \rho v^2 & -2c_{14}b & (c_{13} + c_{44})b & 0 \\ -2c_{14}b & c_{66} + c_{44}b^2 - \rho v^2 & -c_{14} & 0 \\ (c_{13} + c_{44})b & -c_{14} & c_{44} + c_{33}b^2 - \rho v^2 & 0 \\ 0 & 0 & 0 & -\varepsilon_{11} - \varepsilon_{33}b^2 \end{pmatrix} \begin{pmatrix} \alpha_1 \\ \alpha_2 \\ \alpha_3 \\ \alpha_4 \end{pmatrix} = \begin{pmatrix} 0 \\ 0 \\ 0 \\ 0 \end{pmatrix}. \quad (6)$$

For the propagation along the $[1\bar{1}00]$ sapphire direction, we find

$$\begin{pmatrix} c_{11} - 2c_{14}b + c_{44}b^2 - \rho v^2 & 0 & (c_{13} + c_{44})b - c_{14} & 0 \\ 0 & c_{66} + 2c_{14}b + c_{44}b^2 - \rho v^2 & 0 & 0 \\ (c_{13} + c_{44})b - c_{14} & 0 & c_{44} + c_{33}b^2 - \rho v^2 & 0 \\ 0 & 0 & 0 & -\varepsilon_{11} - \varepsilon_{33}b^2 \end{pmatrix} \begin{pmatrix} \alpha_1 \\ \alpha_2 \\ \alpha_3 \\ \alpha_4 \end{pmatrix} = \begin{pmatrix} 0 \\ 0 \\ 0 \\ 0 \end{pmatrix}. \quad (7)$$

Because of the non-piezoelectricity of c-sapphire ($e_{ijk}=0$), the potential component is decoupled from the elastic components for any propagation direction. The piezoelectric coupling in the heterostructures takes place in the GaN overlayers. Equation (6) demonstrates that all the three polarizations are generally mixed for an acoustic wave propagating along the $[11\bar{2}0]$ direction of trigonal crystals because of the non-zero value of c_{14}. A comparison between Eqs. (6) and (7) reveals that the anisotropic acoustic properties in the c plane of trigonal crystals also originate from c_{14} not being zero.

To examine the polarization mixture when a GaN film and sapphire are stacked as a layered system, we show in Figs. 5 and 6 typical examples of the depth profiles of u_j and ϕ for individual surface modes. The displacements u_1, u_2, and u_3

are the longitudinal, shear horizontal, and shear vertical components, respectively. The parameter is $kH \approx 1$ in Fig. 5 and $kH = 6$ in Fig. 6. The suggestions by Eqs. (6) and (7) that sagittal waves and SH waves are coupled when the propagation is along the $[11\bar{2}0]$ direction of trigonal crystals and are decoupled for the propagation along the $[1\bar{1}00]$ direction are indeed found to be the case for the R, S_i, and PB_i modes. These modes exhibit a conventional polarization for the propagation along the $[1\bar{1}00]$ direction, i.e., the acoustic vibration is restricted in the sagittal plane. In contrast, u_2 is non-zero for the propagation along the $[11\bar{2}0]$ direction, i.e., the modes present mixed polarization induced by the sapphire substrate. We note that the depth profiles for the S_1
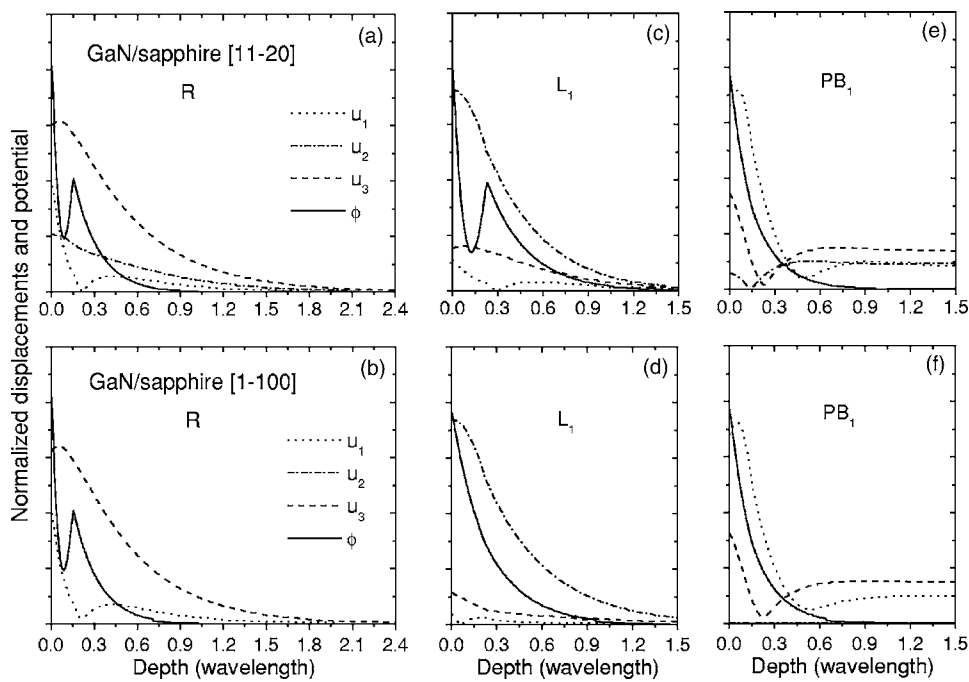
FIG. 5. Normalized particle displacements, u_i, and potential, ϕ, when $kH = 0.94$. The modes are Rayleigh (R), (a) and (b), first Love (L_1), (c) and (d), and first pseudobulk (PB_1), (e) and (f). The propagation is along the $[11\bar{2}0]$ direction for the upper panels and the $[1\bar{1}00]$ direction for the lower panels. The displacements u_1, u_2, and u_3 are the longitudinal, shear horizontal, and shear vertical components, respectively.

mode strongly depend on kH. They are similar to those of the R mode when kH is small. With increasing kH, however, the displacement profile develops structures within the overlayer due to the acoustic confinement, as shown in Fig. 6 for $kH = 6$. It may also be noteworthy that the displacements of the PB_1 mode spread deep into the substrate because of its par-

FIG. 6. Normalized particle displacements, u_i, and potential, ϕ, of the first Sezawa (S_1) mode when $kH = 6$. The propagation direction is (a) $[11\bar{2}0]$ and (b) $[1\bar{1}00]$ of the sapphire substrate. The displacements u_1, u_2, and u_3 are the longitudinal, shear horizontal, and shear vertical components, respectively.

tial coupling with bulk waves, presenting a predominant longitudinal-wave character.

Concerning the L_1 mode, one finds that the polarization mixture takes place for the propagation along both the $[11\bar{2}0]$, Fig. 5(c), and $[1\bar{1}00]$, Fig. 5(d), directions. It is, therefore, indicated that the boundary conditions at the hetero-interface lead to polarization mixture for the SH waves which is not present in the individual components of the layered system. The nonzero sagittal displacements allow the excitation of the L_i modes using IDTs. Since the polarization mixture for the $[1\bar{1}00]$ direction is caused by secondary effects, the sagittal displacements are markedly small in comparison to those induced by the principal effect for the $[11\bar{2}0]$ direction. This explains the difference in the excitation intensities between the two propagation directions observed experimentally in Figs. 1 and 2. Notice that the experimental observation of the L_i modes in Fig. 3 is limited to the region in which the dispersion curves of the R (S_i) and L_i modes are close to each other. The mode coupling is expected to be strong in such a region. Although a number of acoustic modes have been shown to exhibit the polarization mixture, it should be emphasized that they nevertheless retain the dominant polarization. This allows the classification of the surface modes in terms of the conventional notation of the R, S_i, L_i, and PB_i modes, as we have done above.

Love modes have been numerically simulated for the nitride films on $4H\text{-}SiC(0001)$ substrates.[22] Since the crystal structures of both the top layer and the substrate are 6mm, the Love modes are piezoelectrically inactive. The nitrides layers on $\gamma\text{-}LiAlO_2(100)$ (crystal class 422) exhibit anisotropic dispersion.[23] Although the presence of the Love modes has been numerically confirmed,[24] they have not been experimentally observed since the polarization mixture does not take place there along the high-symmetry directions. The use of c-sapphire as the substrate thus provides a unique
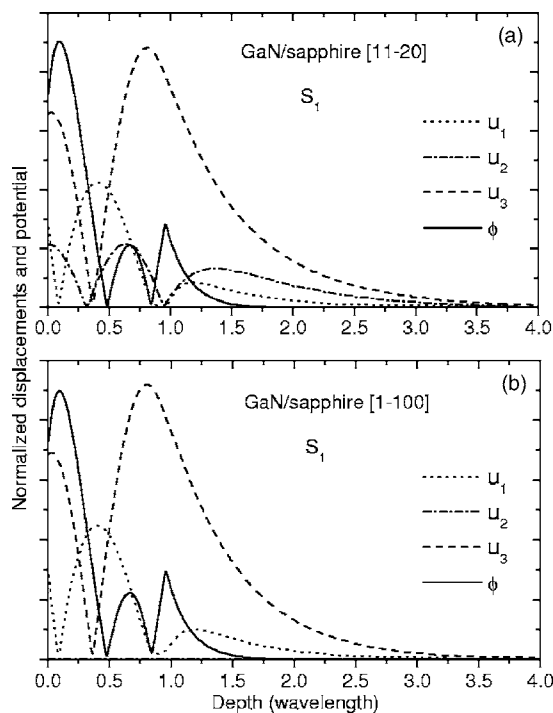
opportunity to excite Love modes using IDTs. R-sapphire, i.e., sapphire $(01\bar{1}2)$, may also permit the Love mode excitation as demonstrated numerically when GaAs[25] or $(Mg)ZnO$[25,26] is the overlayer. In general, the Love-mode excitation along high-crystal-symmetry directions through the polarization mixture is expected to be possible in any layered structures involving trigonal crystals, such $LiNbO_3$, $LiTaO_3$, quartz, and $AlPO_4$.

Shear horizontal waves are useful for SAW-based liquid sensor applications due to the low attenuation of these waves in contact with a fluid, in contrast to the complete damping of the Rayleigh-type modes. The chemical inertness of the nitride films and the Love mode generation enabled by the sapphire make the GaN/sapphire structure a prospective candidate for this purpose. Additionally, the anisotropic propagation offers new capabilities for multichannel sensor designs. Moreover, the convenient excitation of Love modes using IDTs can be exploited in manipulating the optical and electronic properties in the direction transverse to the propagation, allowing us to overcome the restriction of the modulation in the sagittal plane for the Rayleigh mode.

IV. CONCLUSIONS

We have investigated the dispersion and the polarization characteristics of various SAWs and pseudo-SAWs in GaN layers grown on *c*-plane sapphire. In addition to the Rayleigh mode, guided modes in the overlayer arise because of the slow acoustic propagation in GaN in comparison to the substrate. The appreciable penetration of these surface waves to the sapphire substrate for small kH values leads to a generic polarization mixture of the acoustic modes even when the propagation is along high-symmetry directions. The mixture has been manifested to enable unusual excitation of Love modes by means of conventional transducers. The anisotropic elastic properties of the sapphire substrates, which are widely used for the epitaxial growth of nitride layers, can be utilized to enhance the functionality of GaN-based devices. One may alternatively regard the GaN/sapphire heterostructures as a piezoelectrical activation of sapphire using GaN overlayers.

*Email address: jpedros@die.upm.es

[1] F. Calle, J. Pedrós, T. Palacios, and J. Grajal, Phys. Status Solidi C **2**, 976 (2005).

[2] J. Camacho, P. V. Santos, F. Alsina, M. Ramsteiner, K. H. Ploog, A. Cantarero, H. Obloh, and J. Wagner, J. Appl. Phys. **94**, 1892 (2003).

[3] T. Palacios, F. Calle, and J. Grajal, Appl. Phys. Lett. **84**, 3166 (2004).

[4] F. Calle, J. Grajal, and J. Pedrós, Electron. Lett. **40**, 1384 (2004).

[5] D. Cyplys, R. Rimeika, M. S. Shur, R. Gaska, J. Deng, J. W. Yang, and M. A. Khan, Appl. Phys. Lett. **80**, 2020 (2002).

[6] C. Caliendo, Appl. Phys. Lett. **83**, 1641 (2003).

[7] G. W. Farnell and E. Adler, in *Physical Acoustics*, edited by W. P. Mason and R. N. Thurston (Academic, New York, 1972), Vol. 9, pp. 35–127.

[8] C. Deger, E. Born, H. Angerer, O. Ambacher, M. Stuzmann, J. Hornsteiner, E. Riha, and G. Fisherauer, Appl. Phys. Lett. **72**, 2400 (1998).

[9] S. Camou, Th. Pastureaud, H. P. D. Schenk, S. Ballandras, and V. Laude, Electron. Lett. **37**, 1053 (2001).

[10] K. H. Choi, H. J. Kim, S. J. Chung, J. Y. Kim, T. K. Lee, and Y. J. Kim, J. Mater. Res. **18**, 1157 (2003).

[11] K. Sezawa and K. Kanai, Bull. Earthquake Res. Inst., Univ. Tokyo **13**, 237 (1935).

[12] X. Zhang, J. D. Comins, A. G. Every, P. R. Stoddart, W. Pang, and T. E. Derry, Phys. Rev. B **58**, 13677 (1998).

[13] A. G. Every, Meas. Sci. Technol. **13**, R21 (2002).

[14] B. A. Auld, *Acoustic Fields and Waves in Solids* (Wiley, New York, 1973), Vol. 1, p. 392.

[15] A. H. Fahmy and E. L. Adler, Appl. Phys. Lett. **22**, 495 (1973).

[16] M. Pereira da Cunha and E. L. Adler, IEEE Trans. Ultrason. Ferroelectr. Freq. Control **42**, 840 (1995).

[17] A. I. Kozlov, Proc. IEEE Ultrason. Symp. **1**, 197 (1995).

[18] M. H. Kuok, S. C. Ng, and V. L. Zhang, J. Appl. Phys. **89**, 7899 (2001).

[19] M. Chirita, R. Sooryakumar, R. Venugopal, J. Wan, and M. R. Melloch, Phys. Rev. B **63**, 205302 (2001).

[20] X. Zhang, M. H. Manghnani, and A. G. Every, Phys. Rev. B **62**, R2271 (2000).

[21] G. Behme and T. Hesjedal, Appl. Phys. Lett. **77**, 759 (2000).

[22] Y. Takagaki, P. V. Santos, E. Wiebicke, O. Brandt, H. P. Schönherr, and K. H. Ploog, Phys. Rev. B **66**, 155439 (2002).

[23] Y. Takagaki, C. Hucho, E. Wiebicke, Y. J. Sun, O. Brandt, M. Ramsteiner, and K. H. Ploog, Phys. Rev. B **69**, 115317 (2004).

[24] Y. Takagaki, E. Chilla, and K. H. Ploog, J. Appl. Phys. **97**, 034902 (2005).

[25] D. Penunuri and K. M. Lakin, Proc. IEEE Ultrason. Symp. **1**, 328 (1972).

[26] N. W. Emanetoglu, S. Muthukumar, P. Wu, R. H. Wittstruck, Y. Chen, and Y. Lu, IEEE Trans. Ultrason. Ferroelectr. Freq. Control **50**, 537 (2003).

[27] R. J. Jiménez Riobóo, E. Rodriguez-Cañas, M. Vila, C. Prieto, F. Calle, T. Palacios, M. A. Sánchez, F. Omnès, O. Ambacher, B. Assouar, and O. Elmazria, J. Appl. Phys. **92**, 6868 (2002).